EXPERIMENTAL/NUMERICAL INVESTIGATION AIRFOIL WITH FLOW CONTROL BY SYNTHETIC JETS

Stephanus M.D. Widjanarko, Immanuel J.A.K. Geesing, Hein de Vries and Harry W.M. Hoeijmakers

University of Twente, PO Box 217, 7500 AE Enschede, the Netherlands
h.w.m.hoeijmakers@utwente.nl

Keywords: *flow control, synthetic jets, experimental fluid dynamics, CFD*

Abstract

The paper deals with the investigation of active aero-fluidic load control for wings. For load control, it is required to adjust the aerodynamic characteristics over a wide range of angles of attack. This can be achieved by adjusting the circulation of the airfoil by introducing synthetic jets with the exit normal to the surface at a location near the trailing edge. The wing investigated numerically and experimentally is an unswept, two-dimensional wing with a NACA0018 section with spanwise slits at $x/c = 0.88$.

Different turbulator tapes have been employed in order to remove the laminar separation bubble which appears for the Reynolds number considered in the present study ($Re = 88,000 - 550,000$). The resulting measured pressure distributions have been interpreted with the help of results from XFOIL. In general, the results have shown a satisfactory agreement.

A parametric study with flow control by synthetic jets has been carried out for $\alpha = 0$ and for $\alpha = 8$ deg., for which at $Re = 165,000$ c_l/c_d is maximal. The study has been performed in the low-frequency regime, i.e. the dimensionless frequency $F^+ = O(1)$. The effectiveness of flow control is investigated for different frequencies and outflow velocities. For the current configuration, the most distinct effect is at low actuation frequency and at high jet strength. The effectiveness of the synthetic jet actuation is observed in a wide range of angles of attack with a minimum drag penalty. Measured Cp distributions have been compared with numerically simulated Cp distributions.

The numerical simulation reveals details of the actuation in modifying the trailing edge flow

giving insight in the induced effect by synthetic jets. Overall, the jet effectiveness is a function the jet strength, actuation frequency and the angle of attack

1 Introduction)

There are two distinct fields in the research of active flow control: flow-separation control and load control.

For flow-separation control, the fluidic jets are mainly devised to delay or prevent the onset of boundary layer separation by altering the momentum balance inside the boundary layer. However, this concept only works effectively at higher angles of attack, i.e. the stall angle of attack α_{stall} is increased. Fig.1(a) illustrates the effect of flow separation control.
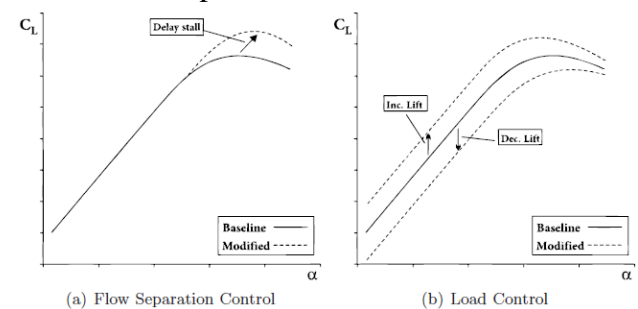

Fig. 1.Effect of flow-separation control and load control on lift curve [1].

For active aerodynamic load control, the use of fluidic jets is different than for flow-separation control. For load control it is required to change the aerodynamic characteristics over a wide range of angles of attack, see Figure 1(b). Hence, the value of c_l can be adjusted at constant pitch angle of the wing. This can be achieved by introducing fluidic jets directed

normal to the surface at a location near the trailing edge, see Fig. 2(a). This creates a region with recirculation near the trailing edge, which will change the angle at which the flow leaves the trailing edge. This effect is similar to the effect of the Gurney flap, see Fig. 2(b). The effect is that the circulation of the airfoil is increased or decreased depending on whether the device is located on the pressure side or the suction side of an airfoil [4], [5]. This type of flow control affects the Kutta condition at the trailing edge of the airfoil. Investigations on load control by other means such as microtabs are found in [3], [4], [1], [6]-[9], by trailing edge flaps in [6], [10].

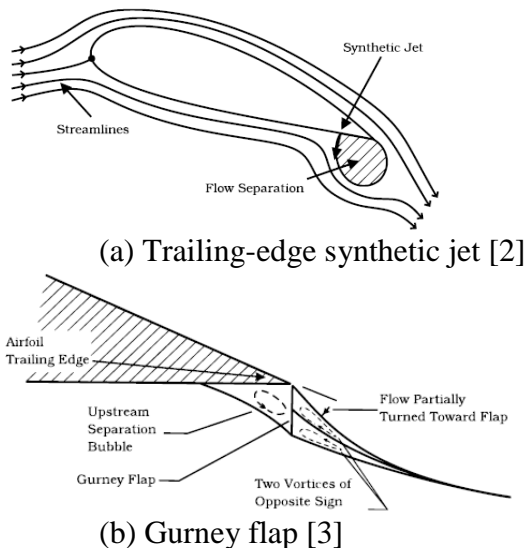(a) Trailing-edge synthetic jet [2]

(b) Gurney flap [3]

Fig. 2. Schematic of trailing edge flow deflection by synthetic jet (a) and by Gurney flap (b)

Regarding the transient response, fluidic load control also shows promising results. It has been shown [4] that 50% of the total increase in lift could be obtained within a time of $tU_\infty/c = 1$, which makes that fluidic load control is a possible option for rapid reaction to gusts encountered by wings or wind turbine blades [5].

Flow control is defined as the ability to alter the character or disposition of a natural flow field actively or passively in order to effect a desired change [11].
Flow control has been investigated thoroughly in a passive or active manner with much focus on the control of flow separation. Apart from the presence of an adverse pressure gradient, a geometrical abnormality like a sharp edge can

be the cause of flow separating. Flow separation is also associated with adverse effects such as loss of lift, increase in drag and loss of pressure recovery.[13] Flow separation may also be accompanied by periodic vortex shedding from the surface of an airfoil which causes pressure fluctuations on the surface of the airfoil and fluctuation in aerodynamic loads. Flow separation control has been addressed by steady means, such as controlling flow separation by steady blowing or suction.
Flow separation takes place in case a low momentum flow is present near the solid surface. For control through suction, the idea is to remove the decelerated fluid near the surface and deflect the high momentum free stream fluid towards the surface. For control through blowing, the injected fluid adds momentum to the retarded fluid within the boundary layer near the surface and therewith delays separation. The fluid may be injected parallel to the wall to increase the shear layer streamwise momentum or normal to the wall to enhance the mixing rate in the boundary layer. For passive flow control, the addition of external energy is not required. Passive flow control by continuous blowing can be realized, for example, through leading-edge slats and trailing-edge flaps which are very common in modern aircraft. This works on the principle of pressure difference between the pressure side and the suction side of the airfoil. Although this leads to a significant increase of the lift, it also introduces a large drag penalty.
Unsteady flow control using periodic excitation has also been investigated in the past decades. This method, which exploits natural flow instability phenomena, has been shown to be more effective than steady flow control [12]. It was also shown in a study that the momentum input to achieve the same result as for the case of steady flow control is smaller by factors or orders of magnitude [14, 15]. Periodic excitation accelerates and regulates the generation of large coherent structures with the flow and hence transfers high momentum fluid across the mixing layer. The invention of synthetic jets opened the possibility for the implementation of fluidic periodic excitation. Synthetic jets are formed by oscillatory flow through an orifice. This means that the fluid injection process con-

sists of both blowing and suction. Synthetic jets use the surrounding fluid as the working fluid while pulsed jet actuation involves a separate working fluid. This unique feature of synthetic jets eliminates the need of additional equipment to realize actuation. In the present study, the possibility of synthetic jets for load control is investigated.

For this purpose a numerical method based on solving the Unsteady Reynolds Averaged Navier Stokes (URANS) equations has been developed. This CFD modeling is validated with the results of the experiments conducted in the silent wind tunnel at the University of Twente. A steady fluidic load control has been performed recently at the University of Twente [5, 15]. The present study investigates unsteady fluidic load control by means of acoustically driven synthetic jets rather than steady fluidic load control.

2 Physical Aspects Unsteady Flow Control
2.1 Periodic Excitation

Flow control utilizing periodic excitation is based on the same principle as steady flow control. Instead of injecting momentum into the boundary layer continuously, momentum is added to and removed from the boundary layer in an oscillatory manner. Periodic excitation is an effective technique to manipulate the flow. Periodic excitation has the potential to be much more effective than steady boundary layer control. Periodic excitation can save momentum addition up to two orders of magnitude compared to steady control methods [12, 13].

The application of periodic excitation with respect to flow separation control is based on the ability to stabilize the boundary layer by adding or removing momentum to or from the boundary layer due to the formation of vortical structures. These vortical structures promote boundary layer mixing and hence momentum exchange between the flow in the outer and the one in the inner (close to the surface) parts of the boundary layer. It is believed that excitation accelerates and regulates the generation of large coherent structures, thereby transfer high momentum fluid across the boundary layer, see Fig. 3. There is a difference between load con-

trol and flow separation control. Load control implies an increase of lift above and below the expected value generated by incidence and camber [14]. Load control can be achieved by changing the flow angle of the flow leaving the trailing edge and thus altering the circulation [1, 5, 16]. Periodic excitation adds more parameters to the challenge compared to steady flow control, both in time and space because effective excitation may trigger instabilities in the flow that increase the strength of the generated vortices that transport the necessary momentum to change the flow.
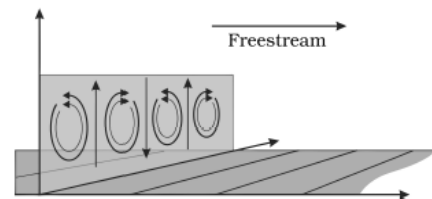

Fig. 3. Mixing inside boundary layer – boundary layer mixing by streamwise vortices. This graph is reproduced from [17]

The local flow field condition proves to be important in flow control effectiveness as studied in [14]. For example for a flapped wing, the actuator is located in the flap shoulder. As the flow separates, the excitation from the flap shoulder becomes ineffective because of the recirculation region in the vicinity of the flap.
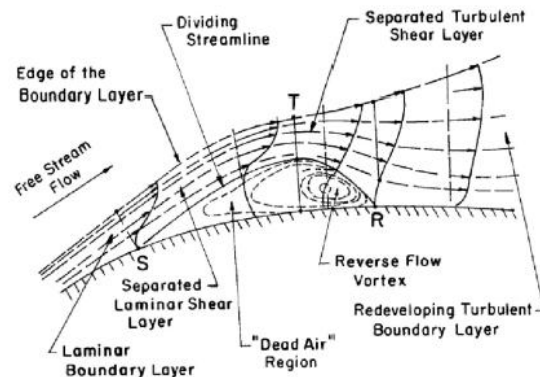

Fig. 4. Laminar separation bubble - Time-averaged structures of laminar separation bubble [19] S: laminar separation point. T: laminar-turbulent transition. R: turbulent re-attachment.

In low-Reynolds-number flow often a laminar separation bubble (LSB) is encountered. The LSB develops when the laminar boundary layer separates just downstream of the point of minimum pressure to form a laminar free shear layer

[18]. If the Reynolds number based on a chord length is greater than 50,000, transition takes place in the separated shear layer and if the adverse pressure gradient is not too large, the flow will reattach to the surface due to the energy recovered from the entrainment in the turbulent shear layer. The time-averaged structure of the laminar separation bubble can be seen in Fig. 4.

The flow with a separation bubble is characterized by instability waves in the upstream laminar shear layer that develop into vortices that are shed at the trailing edge of the bubble. These phenomena cause changes in the excitation frequency, the excitation level and the location of the LSB. Therefore, the presence of a laminar separation bubble considerably complicates the mechanism of flow control.

2.2 Dimensionless Numbers

The Reynolds number, Re, is defined as:

$$\text{Re} \equiv \frac{\rho_\infty U_\infty c}{\mu_\infty} = \frac{U_\infty c}{\nu_\infty} \tag{1}$$

where ρ_∞ is the density of the fluid, U_∞ is the characteristic velocity of the flow, c is the characteristic length scale, μ_∞ is the dynamic viscosity and ν_∞ is the kinematic viscosity $\nu_\infty = \mu_\infty/\rho_\infty$. In the present wind-tunnel experiments the Reynolds number is within the range of 0.88×10^5 to 5.5×10^5, which is considered to be low Reynolds number flow. Typical Reynolds numbers for wings are much higher, 10^7 to 10^8. For such conditions, the flow is laminar on only a small part of the airfoil and turbulent on the most part of the airfoil. In low Reynolds number flows around airfoil sections often a laminar separation bubble appears near the leading edge. In addition, it must be remarked that numerical simulation of flows with a laminar separation bubble is very challenging, a challenge that is avoided here. Therefore, we want to avoid this difficulty in the experiments. This is achieved using turbulator tapes, placed in the leading edge region. These forces the laminar boundary layer to transition into a turbulent boundary layer and prevents the occurrence of a laminar separation bubble.

The Mach number is defined as

$$M_\infty \equiv \frac{U_\infty}{a_\infty} \tag{2}$$

where a_∞ is the speed of sound. The Mach number dictates whether or not compressibility effects play an important role in the flow. For the present experimental study the Mach number is smaller than 0.2, i.e. the effects of compressibility will be negligible.

The actuation frequency f of the periodic excitation is non-dimensionalized using the characteristic length c and characteristic velocity U_∞, i.e.

$$F^+ \equiv \frac{fc}{U_\infty} \tag{3}$$

F^+ relates the period of the actuation cycle to the advection time over the chord of the airfoil.

The performance of the actuator is characterized by the amount of momentum added to the flow. This is defined in dimensionless form as:

$$c_\mu \equiv \frac{\bar{J}}{\frac{1}{2}\rho_\infty U_\infty^2 c} \tag{4}$$

Here $\bar{J}$ is the time-averaged momentum added to the flow, which is defined as:

$$\bar{J} = \frac{W}{\tau_b} \int_0^\tau \rho u(t)^2 \, dt \tag{5}$$

where W is the width of the orifice, ρ and u are the density and the velocity at the orifice, respectively. τ_b is the duration of the outstroke (blowing)period. An alternative and simplified way to characterize the performance of the synthetic jet can also be employed: the velocity ratio, VR. It expresses the ratio between the RMS velocity of the jet at its exit, V_{RMS}, and the free-stream velocity, U_∞:

$$VR \equiv \frac{V_{RMS}}{U_\infty} = \frac{1}{U_\infty}\sqrt{\frac{1}{N}\sum_{i=1}^N u_i^2} \tag{6}$$

with N the number of samples per period.

2.3 Synthetic Jets

The use of zero-net mass flux actuators such as synthetic jets provides beneficial possibilities for the implementation of active flow control. Because the jet is formed entirely from the

working fluid, synthetic jets eliminate the complex piping and fluidic package that is required for the implementation of a continuous jet actuation. Synthetic jet interaction in a quiescent environment and in the presence of a cross flow will be described briefly.

An isolated synthetic jet is produced by the interaction of a train of vortices that is typically formed by alternating momentary ejection and suction of fluid through an orifice [19]. The train of vortices exists because of the flow separating from the edges of the orifice. Following the flow separation at the edge, a vortex sheet is formed which rolls up into a concentrated vortex (vortex ring or vortex pair for circular or two-dimensional jet, respectively), see Fig. 5. Synthetic jets could be generated by an acoustic field, a piston and bellow mechanism or a vibrating diaphragm.
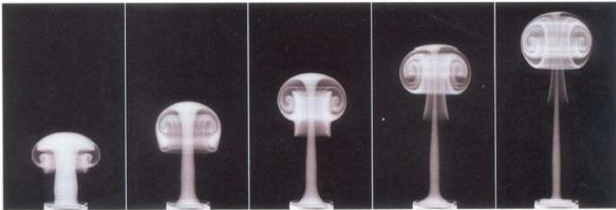

Fig. 5: Vortex development – Evolution of a synthetic jet vortex from a circular orifice. Taken from freshscience.org.au/?p=1541, accessed on Sept 27, 2011.
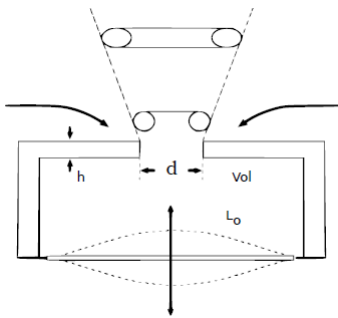

Fig. 6. Schematic of synthetic jet actuator with relevant parameters [21]

The schematic of the synthetic jet actuator with a circular orifice is illustrated in Fig. 6. For non-circular orifices, the aspect ratio of the orifice may influence the out-of-plane distortion of the vortices and the streamwise advection and evolution. The vortex rings may be characterized by a primary parameter which is based on a 'slug' model: the dimensionless stroke length.

$$Stroke - length = \frac{L_o}{d} = \frac{1}{d}\int_0^\tau u_o(t)dt \qquad (7)$$

where $u_o(t)$ is the streamwise velocity averaged over the orifice, τ_o is the time of the discharge and d is the characteristic length scale of the orifice, respectively. In the near field, the vortex evolution depends on the details of the formation and advection of the discrete vortices in the presence of the time-periodic reversed flow. In the far field, the behavior is closer to that of a conventional turbulent jet. For $L_o/d < 3$, the thrust produced by the synthetic jet is smaller than the momentum flux of the ejected fluid. This may be due to the re-ingestion of some of the vorticity formed earlier during the suction stroke. For $L_o/d > 3$, the thrust is equal to the momentum flux of the ejected fluid. Velocity spectra of synthetic jets are characterized by rapid attenuation of the spectral components at frequencies above the formation frequency, which indicates strong mixing and dissipation within the jet and reduction of the turbulence kinetic energy.

2.4 Synthetic Jet in Cross-flow

The interaction of synthetic jets with the cross flow will displace the local streamlines and create a virtual change of the airfoil shape. A study [21] has shown that when the jets are operated on a timescale that is below the characteristic timescale of the base flow, an interaction zone is formed near the surface: a large quasi-steady recirculation zone downstream of the jet. This effect is commonly known as virtual aeroshaping since it effectively increases the camber of the airfoil. The interaction of the jet with the cross flow depends on the dynamic pressure ratio (jet to the cross flow, $(V_{jet}/U_\infty)^2$ and the Strouhal number fW/U_∞. The product of the Strouhal number and the dynamic pressure ratio, i.e. $\hat{f}$ a dimensionless frequency, can be used to divide the flow regime. The critical value $\hat{f}$ is around 0.1 [19]. Below the critical value, discrete vortices form while above the critical value a closed recirculation zone forms. The length of the recirculation zone is proportional to VR and inversely proportional to the upstream boundary

layer thickness. The vortex pairs from the jet interact with the wall boundary layer to form a train of clockwise (CW) vortical structures which convect downstream. This indicates that the upstream CCW jet vortex is accelerated above and around the CW vortex and rapidly weakens. The characteristic time scale of the actuation determines its effectiveness [22–24]. The actuation frequency is directly coupled to the instability mechanisms of the separating shear layer. Large scale vortices are created which increase the entrainment rate and deflect the separated shear layer towards the surface. The actuation frequency is effective for flow separation control if it is of the order of the unstable frequency of the base flow, i.e. $F^+ \sim \mathrm{O}(1)$. Actuation frequencies that are an order of magnitude larger than the characteristic frequency of the airfoil, i.e. $F^+ \sim \mathrm{O}(10)$, can be used for virtual aeroshaping. However, the effect on the aerodynamic properties at such a high frequency has not yet reached a general consensus. One argues that the interaction zone between the actuator and the cross-flow is invariant to the mean time scale of the flow and therefore global aerodynamic properties could be considered constant and decoupled from the operating frequency of the actuators [23]. Other authors argue that high actuation frequencies generate a lower growth rate of the vorticis in the jet, thus will have no positive effect on separation control [24].

2.5 Synthetic Jet Actuators

A review of possible actuators for active flow control is discussed in detail in reference [20, 44]. Here a brief overview is given.

Acoustic
Several researchers use an acoustic driver to generate synthetic jets [15, 22, 23, 25, 26]. In general speakers are not capable to produce the high pressure fluctuations which are needed to achieve a high jet velocity. Furthermore, due to the size of the speakers, it is not easy to place the actuators inside the plenum of an airfoil. Instead, most researchers place the speakers on both ends of the airfoil. For such a configuration it is difficulty to produce a uniform jet in the spanwise direction along the slit, especially at high frequency. Attention has to be paid to the ratio of the slit length and the wavelength of the acoustic field in order to obtain a reasonable uniform velocity along the span of the slit. This limits the maximum frequency attainable from acoustic drivers. Acoustic drivers are generally optimum to synthetic jets up to 200 Hz, i.e. for the low frequency regime.

Piston
A reciprocating mechanism as a way to produce synthetic jets has proven to be effective to produce synthetic jets [27–29]. High ejection velocities up to 125 m/s can be achieved using the reciprocating mechanism. The maximum frequency obtained by a piston actuator depends on the motor but in general it is applied in the low frequency regime. With an appropriate design, it is possible to decouple amplitude from the frequency of the actuation.

Vibrating Diaphragm
A compact actuator can be constructed employing a vibrating diaphragm. Several researchers use a piezoelectric diaphragm to obtain synthetic jets [30, 31, 32, 22, 23, 33, 34]. Due to the small and compact size of the actuator, it is possible to place the actuator inside the plenum of the airfoil. Piezoelectric actuators are capable to handle very high frequencies up to 1800 Hz, which is very suitable for investigating the high frequency regimes. However, piezoelectric actuators are generally not capable to produce a high amplitude velocity due to the small displacement of the diaphragm.

Valves
Several researchers in the field of flow control choose to use valve type actuators. A synthetic jet can be produced by means of a rotating valve without the need of a vacuum chamber [35, 36]. A solenoid valve can also be used to generate synthetic jets. However, it requires a vacuum pump for the suction part of the cycle [2, 26, 37, 38]. High pressure supply systems are required, which contrasts the idea to form jets using the working fluid only. The maximum frequency from the valve type of actuators is around 800 Hz which is suitable for investigations at low to medium frequencies.

3.   Experimental Set-up

The wind tunnel facility will be described as well as the wind tunnel model (i.e. airfoil). Furthermore, the synthetic jet excitation system will be presented. Finally, the utilized measurement equipment is described.

3.1.   Experimental Facility

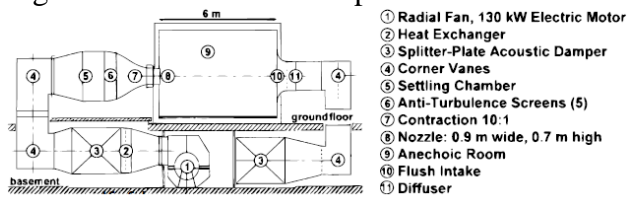The experiments have been conducted in the closed-loop Twente Silent Wind Tunnel, see Fig. 7 for a schematic set-up.

Fig. 7. Schematic of closed return wind tunnel at the University of Twente

The wind tunnel test section, attached to the nozzle (number 8 in Fig. 7), is 0.7 m high, 0.9 m wide and 2.25 m long. The wind tunnel is powered by a 130 kW electrical motor. The maximum velocity is $U_\infty = 70$ m/s in the test section. The temperature of the air at the test section is maintained constant by the controllable heat exchanger located downstream of the fan. The settling chamber features 5 screens to reduce the turbulence intensity of the airflow. The contraction ratio of the nozzle connecting the settling chamber to the test section is 10:1. The anti-turbulence screens in combination with the contraction result in a low level of free-stream turbulence of 0.4 % up to a free-stream velocity of 50 m/s in the test section, see [44]. Tests have been conducted at Reynolds numbers ranging from 0.88×10^5 to 5.5×10^5. The free-stream Mach number ranges from 0.02 to 0.147.

3.2.   Wind-tunnel Model

The model investigated is the NACA 0018 airfoil section. This is a symmetrical airfoil with a thickness to chord ratio of 18%. The chord length and span of the model is 0.165 m and 0.9 m, respectively. For a schematic of the test sec-

tion, see Fig. 3.2. The setup is two-dimensional, i.e. the wing spans the test section, resulting in an aspect ratio of 5.45 in the wind tunnel but an aspect ratio of infinity aerodynamically. The aspect ratio of 5.45 is larger than that of the wind tunnel model in [37, 38]. A larger aspect ratio reduces the disturbance from the wind-tunnel sidewall boundary layer. This is essential for high lift conditions because a significant chordwise pressure gradient is created that can disturb the sidewall boundary layer. The model is equipped with 29 pressure taps distributed over its upper and lower surface. The model is a single piece extruded aluminum with three separate internal cavities, see Fig. 8.
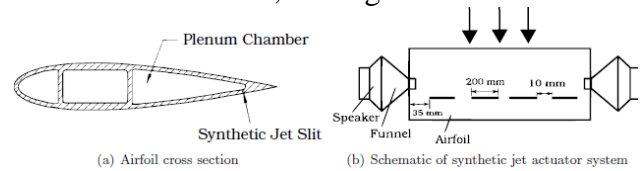

Fig. 8. Synthetic jet actuator system. Sketch is not to scale.

The aft compartment is used for synthetic jet actuation. Four rectangular slits with a width of 1 mm (W/c = 0.00606) and a length (spanwise) of 200 mm are located at x/c = 0.88. The spanwise distance between each slit is 10 mm. A previous study has indicated that the two central slits perform best in terms of spanwise flow uniformity and jet strength [39]. The jets exit perpendicularly to the surface of the airfoil.

To fix the transition location and to guarantee a turbulent boundary layer along the airfoil, a zig-zag tape is located on both sides of the airfoil at x/c = 0.06. This is intended to eliminate the Laminar Separation Bubble (LSB) that appears in case the boundary layer is laminar. Locating the laminar to turbulent transition close to the leading edge conforms to the situation encountered in high-Reynolds-number flow. It also reduces the complexity of the flow making the comparison with numerical simulations is more straightforward. The location and the thickness of the turbulator tapes are based on the previous study [40]. The (Streifeneder) zig-zag tape with thickness of 0.4 mm, width of 6 mm and 70 deg zig-zag angle eliminated the LSB for free-stream velocities larger than 16 m/s, i.e. for Reynolds numbers above 165,000, see [44].

3.3. Excitation System

The rear cavity of the airfoil is used as a plenum chamber to produce a synthetic jet exiting at x/c = 0.88 on the lower side of the airfoil. The oscillating pressure required to produce a synthetic jet is provided acoustically using a pair of high-quality JBL (2206H/J) speakers mounted on each side of the airfoil through funnel adapters that match the diameter of the speaker diaphragm to the height of the plenum, see Fig. 8. The speakers are rated at nominally 600W peak power with a good response at low frequencies, down to about 40 Hz. A two-channel, 500 W power amplifier type QSC (RMX2450) at 8 Ω rated impedance of the speaker is used to power the speakers in parallel. The sinusoidal signal is produced by NI PXI-1042 from National Instrument.

Characterization of the synthetic jet actuator system, in work-bench experiments, using hot wire measurements has been performed in a previous study [39]. Two frequencies (15 Hz and 100 Hz) have been studied extensively both in terms of the jet strength and its spanwise variation. Although a frequency of 15 Hz is lower than the specified range of accurate frequency response of the speakers, the jet does not show severe distortion. It is also concluded that two slits perform better than four slits in terms of spanwise jet uniformity and jet strength. The jet tends to become less uniform in spanwise direction as the frequency of the actuation becomes higher. The previous study also concluded that the maximum jet velocity during the outstroke cycle reaches a value up to 60 m/s.

In the present study, the root mean square of the jet velocity, V_{RMS}, is used to quantify the momentum addition to the flow. The jet velocity is measured using hot wire anenometry one slot width above the jet exit surface. The hot wire is located directly above the middle of the slit. Other studies have used the outstroke part of the jet to quantify momentum addition to the flow [22, 41], the maximum jet velocity [27, 28] or the mean jet velocity [33].

To investigate the global aerodynamic characteristics, five different frequencies 15, 25, 50, 75, 100 and 120 Hz have been used to excite the speakers.

3.4. Pressure measurement

Two pressure scanners from Esterline (9816-6496 and 9816-6498) are used for recording the pressure distributions on the airfoil. Esterline 9816-6498 is capable of handling a maximum pressure up to 7 kPa and is connected to the pressure taps on the top surface of the airfoil whereas Esterline 9816-6496 is capable to handle a maximum pressure up to 17 kPa and is connected to the pressure taps on the bottom surface of the airfoil. These pressure scanners can resolve pressures down to 0.5 Pa (9816-6498) and 0.2 Pa (9186-6496), respectively. Furthermore, they employ piezo-resistive pressure sensors which have build-in temperature sensors to perform automatic temperature compensation and to maintain an acceptable level of zero-drift after scanners have been re-zeroed before each measurement.

3.5. Hot-wire Anemometry

The velocity distribution in the jet has been measured using hot wire anemometry (HWA). HWA has also been used for determining the free stream turbulence intensity. A Dantec Stream-Line measuring system operated in constant temperature mode is used. The entire system is connected to a personal computer for data acquisition and analysis.

A single normal Dantec hot wire probe (55P11) with tungsten wire is employed. This hot wire has a probe length l_w = 1.2 mm and diameter d_w = 5 μm. The hot wire probe is connected to a Dantec (90C10) module to control the temperature. This module is then connected to a 16 bit A/D board from National Instrument (AT MIO 16EI). Afterwards, the sampled data is transferred to the personal computer using Dantec Streamware software. The sampling rate is set at 25 kHz for both free-stream turbulence intensity measurements and synthetic jet measurements. Low pass filtering is applied at 10 kHz.

4. Results Wind Tunnel Measurements

The set-up of the HWA in the wind tunnel is shown in Fig. 9.

Fig. 9. Model with hot wire positioned above slit

4.1 Results for Zero Free-StreamVelocity

Using the HWA system the strength of the synthetic jet has been determined in terms of the root mean square velocity V_{RMS} as well as the peak jet velocity V_{peak} at one slit width above the middle of the slit. The data is sampled at a sampling frequency of 25 kHz with 1×10^6 samples.
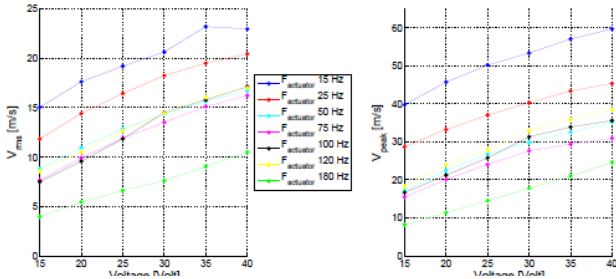

Fig. 10. Synthetic jet strength as a function of input power. $U_\infty = 0$. Left: V_{RMS}. Right: V_{peak}.

The root-mean-square velocity VRMS and the peak velocity V_{peak} as a function of the input voltage are shown in Fig. 10. Both velocities increase almost linear with applied voltage for all frequencies considered. The highest obtainable (peak) velocity of 60 m/s is observed for the lowest frequency. The velocity that the actuator achieves drops as the frequency increases. In the range between 50 Hz and 120 Hz there is not much variation with frequency. The value drops significantly at the highest frequency (180 Hz). It is presumed that the reason is that at the higher frequencies the amplitude of the pressure wave is reduced because energy is partially dissipated through the slit. As the excitation wave-

length is decreased by increasing the excitation frequency, the slit length becomes a larger fraction of the wavelength which results in a larger phase shift as the pressure waves travel along the airfoil plenum. Hence, the issuing jet velocity drops at high frequency and the jet is less uniform across the span.
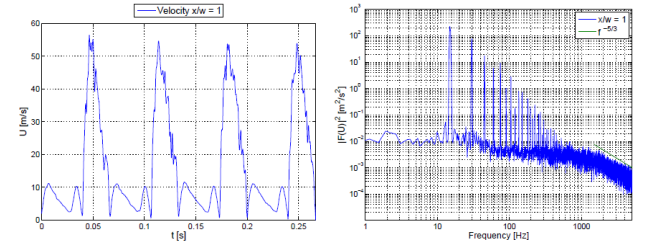

Fig. 11. Measured velocity in synthetic jet for 15 Hz and 40 V. $U_\infty = 0$. Left: time domain. Right: frequency domain

Fig. 11 shows the time and frequency domain plot for the synthetic jet actuator operating at 15 Hz and 40 V. The reversal of the direction of the flow during the suction cycle cannot be resolved using the HWA technique applied in the present study. As a consequence, the time domain signal is rectified during the suction part of the cycle. At this lowest frequency measured, the time domain signal is distorted during the suction stroke. One possible explanation is that 15 Hz is below the lowest optimum frequency response for this specific acoustic driver which is 40 Hz. This distorted signal is not observed when the actuation frequency is in the optimum frequency response of the speaker, as shown in Fig. 12 for actuation frequency of 75 Hz.
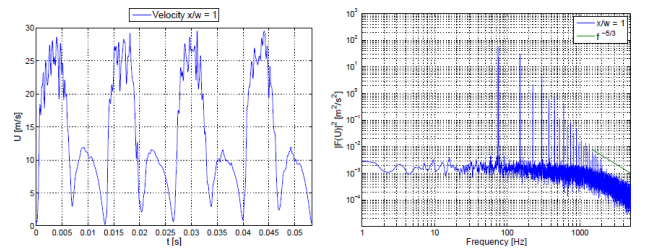

Fig. 12. Measured velocity in synthetic jet for 75 Hz and 40 V. $U_\infty = 0$. Left: time domain. Right: frequency domain

Additional insight into the synthetic jets is gained from the spectral plot of the jet velocity, included in Figs. 11 and 12. The spectrum is dominated by the formation frequency of the jet

and its higher harmonics. The signal rectification due to the HWA also contributes to the higher harmonics as has been observed in other studies [25, 42] as well. There is no evidence of sub-harmonics present at this measurement location. This is a typical synthetic jet evolution for which the absence of pairing interactions between the vortex pairs leads to the absence of sub-harmonics in the spectral plot [34, 42]. Below the fundamental frequency, the spectral distribution is virtually featureless. The spectral plots have a region in which the energy decays as $f^{-5/3}$ which shows that the jet has become turbulent. The present result is a spectral plot obtained from the measurement in still air that is similar to that obtained in other studies. The plot exhibits that turbulent synthetic jets are formed by the present configuration. Other methods to investigate whether synthetic jets form or not are available in the literature. In reference [19], the jet formation criterion is from the dimensionless stroke length and Strouhal number based on the orifice width. A small dimensionless stroke length (~ O(0.1m)) and large Strouhal number (~ O(1)) fail to generate synthetic jets. In another reference [25], the jet formation criterion is based on $1/Sr > K$, where K is approximately 2 for a nominally two-dimensional synthetic jet. At the highest frequency of actuation (180 Hz) and the lowest root-mean-square velocity measured (V_{RMS}) in which Strouhal number based on the width of the orifice is expected to be the largest in the measured data set, the value of $1/Sr$ is approximately 22. This value emphasizes that synthetic jets indeed have formed in the present configuration.

4.2   Experimental Results for Load Control

The purpose of the measurements is to determine whether synthetic jets located at x/c = 0.88 can affect the circulation of the airfoil and therewith its lift. The slit is located on the bottom side of the airfoil. For positive angles of attack this implies that the slit is located on the pressure side of the airfoil. Therefore, it is expected that the effect of the synthetic jet is to increase the circulation of the airfoil and thus shift the lift curve upward in the linear part of the lift curve.

The hot wire setup is placed in the test section during the parametric study in order to determine the behavior of the synthetic jet in the presence of the cross-flow. The achieved performance in cross-flow can then be compared with the performance for the case of still air.

Static pressure measurements have been performed with the 0.4 mm thick turbulator strip placed at $x/c = 0.06$ on both surfaces of the wing. The measurements have been performed at a tunnel speed of 16 m/s, which corresponds to the Reynolds number of 165,000 and a Mach number of 0.045. The full measurement matrix for the parametric study is shown in Table 1.

Geometric α	Actuation Frequency	Velocity Ratio
0°	f:15 Hz - 120 Hz $\rightarrow F^+$:0.16 - 1.28	~ 1
8°	f:15 Hz - 120 Hz $\rightarrow F^+$:0.16 - 1.28	~ 1
8°	f:25 Hz $\rightarrow F^+$:0.27	0.5 - 1.6
8°	f:15 Hz $\rightarrow F^+$:0.16	0.8 - 1.5
-8°	f:15 Hz - 120 Hz $\rightarrow F^+$:0.16 - 1.28	~ 1
0° to 14°	f:15 Hz $\rightarrow F^+$:0.16	~ 1.5

Table 1. Test matrix for parametric study

The momentum coefficient c_μ is calculated using Eqs. 4 and 5. The domain data is separated in the suction stroke τ_s and the blowing stroke τ_b, see Fig. 13.
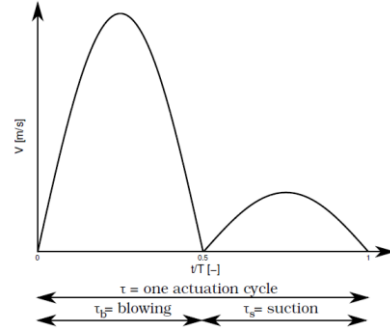

Fig. 13. Splitting of the rectified HWA signal in blowing and suction part of a cycle

The blowing part of the cycle is then integrated to obtain the momentum coefficient. This process is repeated over several cycles and then averaged to get the mean momentum coefficient, see [44] for more details.

The thickness of the boundary layer at the location of the slit is estimated from the boundary-layer displacement thickness obtained from XFOIL.

To assess the effectiveness of the synthetic-jet actuation the increment of the lift coefficient is

determined from the measured surface pressure distributions. The resulting lift coefficient difference Δc_l is then divided by the lift slope of the measurement without actuation at 16 m/s (i.e. $dc_l/d\alpha = 0.09$ per deg.) in order to get a merit number for the pitch angle change due to the synthetic jet actuation. This gives:

$$\Delta\alpha = [c_l(VR, F^+) - c_l(0,0)] / \frac{dc_l}{d\alpha} \qquad (8)$$

4.2.1. Lift Enhancement for $VR \approx 1$, $\alpha = 0$

The variation of the increment of the pitch angle $\Delta c_l/(dc_l/d\alpha)$ as function of frequency F^+ at a fairly constant velocity ratio VR, is shown in Fig. 14. The hot wire signal without and with the free stream are shown in Fig. 15. Both the time domain and the frequency domain are presented in order to gain more insight.
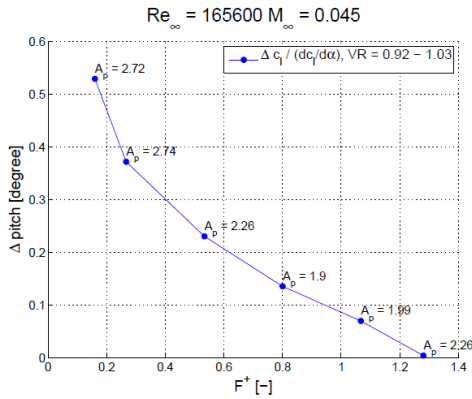
Fig. 14. $\Delta\alpha$ as function of F^+ at about constant velocity ratio $VR \approx 1.0$. Indicated is peak velocity ratio A_p. $U_\infty = 16$ m/s and $\alpha = 0$.

As seen clearly from Fig. 14, for the range of F^+ investigated, the effectiveness of the pitch angle control decreases as F^+ increases for a velocity ratio VR of about 1.0, with a variation of about 10%. Note that the amplitude ratio $A_p \equiv V_{peak}/U_\infty$ is indicated in the plot. The value of A_p varies more along the curve than VR. This is inherent for the present implementation of the actuator mechanism in the wind-tunnel model. The highest pitch angle increment is observed at the lowest actuation frequency, corresponding to $F^+ = 0.16$ for which the pitch angle increment is approximately 0.5 deg. At higher frequencies, the effectiveness of the pitch angle control decreases and a value close to zero is found at the

highest actuation frequency considered. Apparently, at higher actuation frequency F^+, the size of the recirculation zone downstream of the orifice becomes smaller and the effectiveness of the jet to entrain fluid from the top side of the airfoil to its lower side decreases.
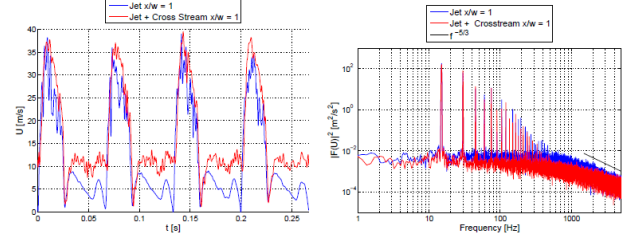

Fig. 15a. Measured velocity in synthetic jet for 15 Hz and 20 V. $U_\infty = 16$ m/s, $\alpha = 0$. Left: time domain. Right: frequency domain
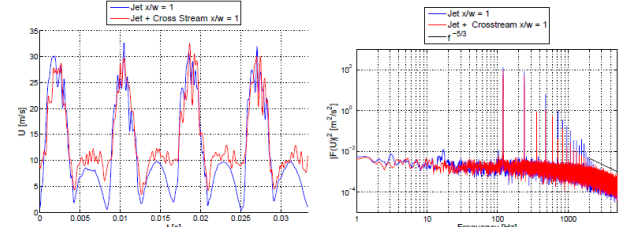

Fig. 15b. Measured velocity in synthetic jet for 120 Hz and 40 V. $U_\infty = 16$ m/s, $\alpha = 0$. Left: time domain. Right: frequency domain

From the HWA data presented in the time domain, the peak velocity observed during the blowing stroke for still air, is similar to the one for the case of $U_\infty = 16$ m/s, both for the lowest actuation frequency (15 Hz) and the highest actuation frequency (120 Hz). During the suction stroke, the effect of the cross stream is more pronounced. The boundary layer thickness estimated from XFOIL for $\alpha = 0$ at $x/c = 0.88$ is in the range of 2.6 mm to 3.9 mm. Due to the suction, the boundary layer thickness might be thinner. However, the hot wire is still located inside the boundary layer as the velocity magnitude during the suction stroke is 3 m/s or 4 m/s lower than the free-stream velocity (16 m/s).

From the spectral plot, the power at the fundamental frequency is not affected very much by the cross-stream at the lowest and the highest actuation frequency measured. The jet is turbulent for both the case of the synthetic jet exiting in still air and the case of the jet exiting in the flow around the airfoil at 16 m/s: in the high frequency range there is a region where the energy decays as $f^{-5/3}$. At the lowest actuation frequen-

cy, the power spectrum above the formation frequency is lower than the power spectrum for the case of still air. However, this is not observed for the highest actuation frequency. The drop of the power spectrum might indicate that the jet mixes with the free-stream flow, which might explain the effectiveness of the pitch angle control at lower actuation frequencies.

4.2.2. Lift Enhancement for $VR \approx 1$, $\alpha = 8$ deg

A similar trend of the pitch control effectiveness is observed for $\alpha = 8$ deg, as shown in Fig. 16.
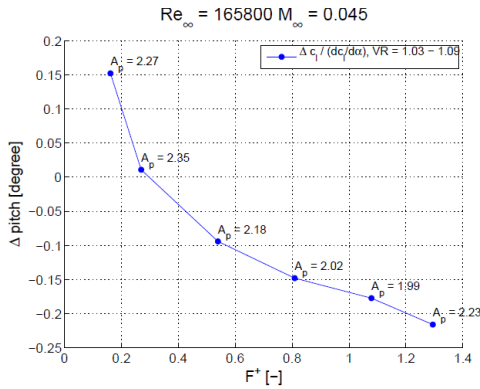
Fig. 16. $\Delta\alpha$ as function of F^+ at about constant velocity ratio $VR \approx 1.0$. Indicated is peak velocity ratio A_p. $U_\infty = 16$ m/s and $\alpha = 8$ deg.

However, within the range of frequencies investigated, the pitch angle control loses its effectiveness and becomes negative for the higher actuation frequencies. The value of the frequency for which the effect is reversed is apparently a function of angle of attack. For $\alpha = 0$ the threshold F^+ is 1.3, while for $\alpha = 8$ deg the threshold is at $F^+ = 0.3$ The most distinct effect of the pitch control is still observed at the lowest actuation frequency, albeit the absolute value is much smaller for $\alpha = 8$ deg than for $\alpha = 0$. This indicates that the local flow state (boundary layer thickness δ) and the actuation frequency determine the strength of the jet-generated recirculation zone, which causes the change of the circulation of the airfoil.

The hot wire signal without and that with the free stream are shown in Fig. 17. During the suction stroke, the velocity magnitude is much larger for $U_\infty = 16$ m/s than for $U_\infty = 0$.
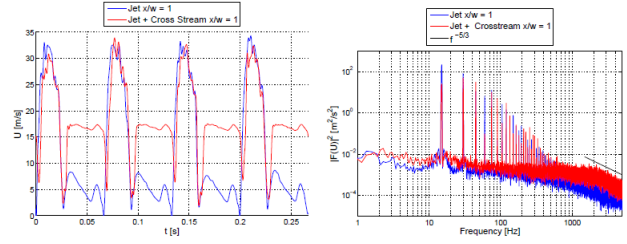

Fig. 17a. Measured velocity in synthetic jet for 15 Hz and 20 V. $U_\infty = 16$ m/s, $\alpha = 8$ deg. Left: time domain. Right: frequency domain
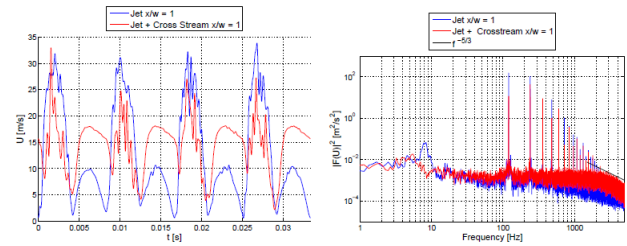

Fig. 17b. Measured velocity in synthetic jet for 120 Hz and 40 V. $U_\infty = 16$ m/s, $\alpha = 8$ deg. Left: time domain. Right: frequency domain

In the former case the suction velocity is of the order of the free-stream velocity (16 m/s). The boundary layer thickness estimated from XFOIL for $\alpha = 8$ deg, at $x/c = 0.88$ is in the range of 1.4 mm to 2.6 mm. Due to the suction the boundary layer might be thinner. It is expected that he hot wire is outside the boundary layer so that the velocity magnitude during the suction stroke is close to the free-stream velocity (16 m/s). For the highest actuation frequency, the blowing stroke is affected by the presence of the nonzero free stream: the peak velocity is strongly decreased. This may explain the failure of the jet to produce the recirculation zone that is required to increase the circulation of the airfoil.

From the spectral plot, the power at the fundamental frequency drops approximately an order of magnitude compared to the case with the free-stream present. Above the fundamental frequency the power spectrum for $\alpha = 8$ deg has now a higher value than for $\alpha = 0$.

4.2.3. Lift Enhancement for $F^+ = 0.16$, $\alpha = 8$ deg

Fig. 18 shows the effect of the jet strength on the control effectiveness for $\alpha = 8$ deg. The measurement has been performed at a constant

actuation frequency ($f = 15$ Hz, i.e. $F^+ = 0.16$). A positive lift increase (i.e. positive delta pitch angle) is observed for all VR's considered. A linear trend is observed up to $VR = 1.3$. For higher values of VR, the lift increase starts to deviate from the linear trend although the lift
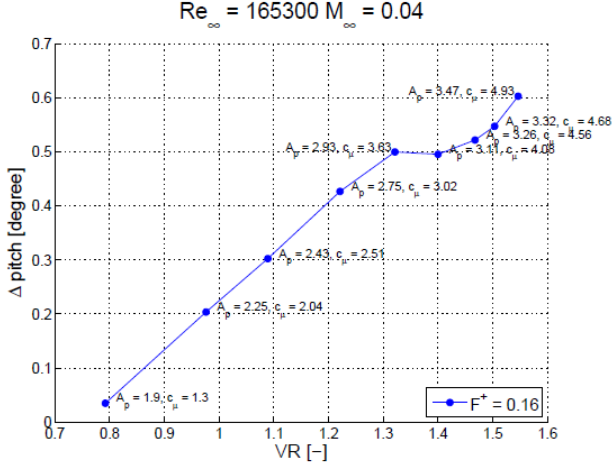

Fig. 18. $\Delta\alpha$ as function of VR at $F^+ = 0.16$. Indicated are peak velocity ratio A_p and momentum coefficient $100c_\mu$. $U_\infty = 16$ m/s and $\alpha = 8$ deg.

keeps increasing for increasing jet strength. The larger pitch angle increment for higher jet strengths indicates that the recirculation zone downstream of the orifice becomes stronger and increases the circulation of the airfoil as the streamlines are deflected downward more. The increase of the recirculation zone as the jet strength increases, at constant actuation frequency, has also been reported in [21].

From Fig. 18 and other results of the present study it follows that the momentum coefficient and amplitude ratio required to have a positive effect is of the order of O(0.04) and O(3) for this specific configuration, respectively. The required momentum coefficient to control the circulation of the airfoil is one or two orders of magnitude higher than the momentum coefficient required to control flow separation, which is of the order of $O(10^{-4} – 10^{-3})$.

4.2.4. Lift Enhancement and Mitigation for $VR \approx 1$, $\alpha = 8$ deg

As shown in Figs. 14, 16 and 18, lift enhancement can be achieved when the jet is located on the pressure side of the airfoil. Lift mitigation can be achieved when the jet is located on the

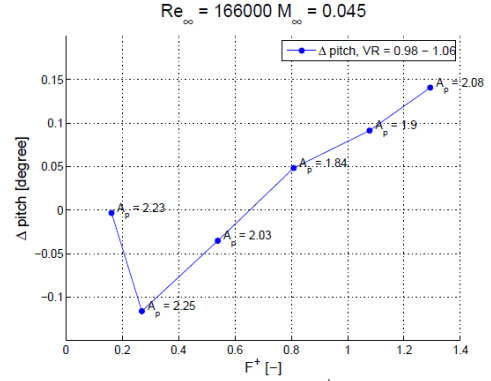suction side of the airfoil, see Fig. 19, for $\alpha = 8$ deg.

Fig. 19. $\Delta\alpha$ as function of F^+ at about constant velocity ratio $VR \approx 1.0$. Indicated is peak velocity ratio A_p. $U_\infty = 16$ m/s and $\alpha = 8$ deg. Actuator on upper side airfoil

Fig. 19 shows that lift mitigation can be achieved indeed with the jet location at $x/c = 0.88$. The lift mitigation is effective at low actuation frequency, similar as for case of lift enhancement, see Fig. 16.

For lift mitigation the present location of the synthetic jet may not be optimum due the nature of the flow for this relatively thick airfoil (NACA0018). For the Reynolds number considered, a trailing-edge type of flow separation is expected to have already occurred at this angle of attack. As with increasing angle of attack, the flow separation region continues to grow, the jet will be engulfed by the recirculation flow, strongly reduces the jet effectiveness to control the circulation of the airfoil. The change of effectiveness due to the local flow state is also observed studies employing a micro-tab located on the suction side for lift mitigation purpose [9]. The different behavior of the jet when located in regions with a different flow state emphasizes that the local flow state affects the effectiveness of the actuator.

Note that for higher F^+, lift enhancement is achieved again. It is thought that actuation at these higher frequencies reduces the separated flow region at the trailing edge, therewith increasing the lift.

4.2.5. Lift as Function of Angle of Attack

Fig. 20 shows the effect of the synthetic jet on the lift as function of attack for $U_\infty = 16$ m/s and jet strength, $VR = 1.51$, $A_p = 3.28$. In the linear regime the synthetic jet, placed at 88% chord on the pressure side, results in an increment in the lift of ~0.06. This effect persists in the pre-stall and post-stall regime. However, the pressure distribution for $x/c > 0.7879$ is not resolved in the measurement and the corresponding contribution in lift is not reflected in Fig. 20.
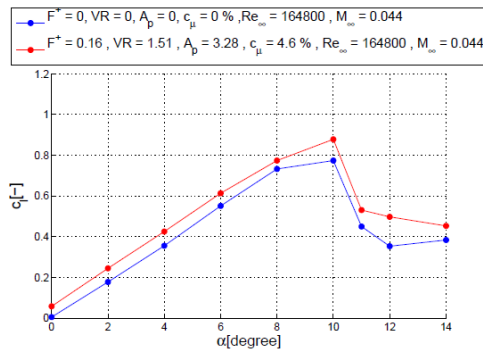
Fig. 20. Lift coefficient as function of incidence, determined from integration surface pressure distribution. Blue: without, red: with actuation. $Re_c = 165,000$, $F^+ = 0.16$, $A_p = 3.28$, $VR = 1.51$

Fig. 21 shows the C_p distribution for $\alpha = 8$ deg corresponding to Fig, 20. The pressure tap on the upper side at $x/c = 0.1$ is partly sealed off by the turbulator strip, so this value is not reliable. The C_p distribution with the synthetic jet active almost coincides with that without actuation at all tap locations. It is evident that the synthetic jet has a global effect on the pressure distribution both on the suction side and on the pressure side of the airfoil.
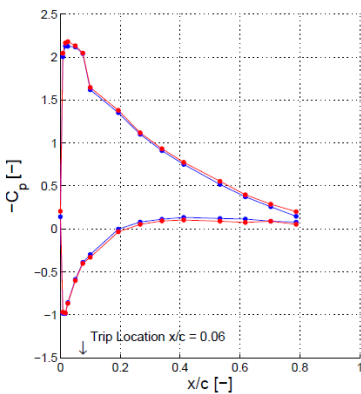

Fig. 21. Pressure coefficient as function of x/c. Blue: without, red: with actuation. $Re_c = 165,000$, $F^+ = 0.16$, $A_p = 3.28$, $VR = 1.51$

4.3 Computational Results for Load Control

A numerical simulation has been performed for the flow around a NACA0018 airfoil at $\alpha = 0$. This numerical simulation provides insight into the flow phenomena near the trailing edge that govern the load control system.

The original NACA0018 airfoil section has a finite trailing edge thickness. Therefore, the trailing edge is extended to zero thickness at $x/c = 1.00893$, and subsequently scaled back to $c = 0.165$. The airfoil is located in the wind tunnel, described in section 3.1.

The inflow velocity is equal to $U_\infty = 16$ m/s, which corresponds to a Reynolds number of 165,000 and a Mach number of 0.045. The actuation frequency is set at 15 Hz corresponding to $F^+ = 0.16$, i.e. a low-frequency, quasi steady condition. The jet strength is set at $A_p = 3.0$.

4.3.1 Computational Domain and Boundary Conditions

The computational domain is sketched in Fig. 22. The airfoil is located in the wind tunnel domain, which extends 20c both in the upstream and the downstream direction. The height of the computational domain is the same as the height of the wind tunnel test section, which is 0.7 m.
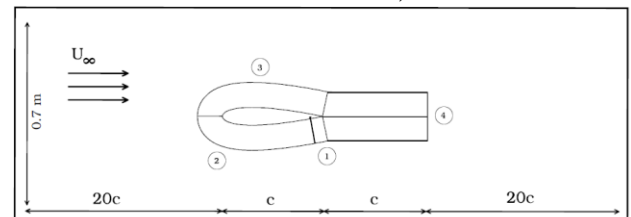

Fig. 22. Computational domain for NACA 0018 at $\alpha = 0$ in wind tunnel. Sketch is not to scale.

A hybrid mesh has been constructed using open source 3D grid generator, *Gmsh* [43]. A prismatic layer is constructed along the airfoil contour and its wake line as indicated with the circled numbers in Fig. 22. The prismatic layer consists of quadrilateral elements and extends 0.25c in the surface normal direction to resolve the boundary layer and the synthetic jet accurately. The region in the wake, number 4, with quadrilateral elements extends 1c downstream of the trailing edge. The rest of the computation-

al domain is filled with triangles. The prismatic layer has 138 points in the normal direction with a stretching ratio of 1.05. The top surface has 171 points, clustered around the leading and trailing edge. The bottom surface has 304 points, including 51 points across the orifice of the synthetic jet. Points are more clustered around the leading edge, trailing edge and the slit. This configuration results in a y^+ value of less than 0.15 for Re = 165,000.
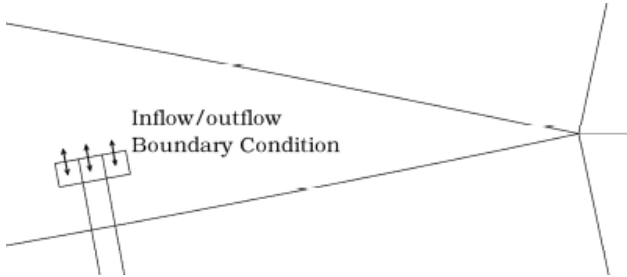

Fig. 23. Close up of computational domain around plenum synthetic jet actuator

For the jet plenum, a small part of the synthetic jet actuator at $x/c = 0.88$ is included in the computational domain, see Fig. 23. The domain includes the slit and a small part of the cavity. The flow inside this cavity is simulated using a customized time-dependent inflow and outflow boundary condition at the bottom of the cavity. With this technique, the jet has time and space to develop. The flow separates at the sharp edges of the orifice resulting in a so-called vena contracta. The grid points are clustered around the sharp edges of the orifice to capture the flow separation. The bottom of the plenum is discretized using 151 points, the two side walls are described by 51 points, the top of the plenum has 51 points on either side of the orifice, while the two walls of the orifice contain 171 points. This grid arrangement results in a total number of elements around 338,000.

The no-slip boundary condition is applied on the airfoil surface. For the top and bottom of the tunnel wall, the slip boundary condition is applied, which avoids having to resolve the boundary layer on these walls. At the entrance of the domain, an inflow boundary condition is prescribed with the free-stream velocity and free-stream density. At the exit of the domain the free-stream pressure is prescribed.

At the bottom of the cavity a harmonic boundary condition is applied, which is a spatially uniform time-dependent in/outflow, i.e. a zero mass flux boundary condition, sinusoidal in time.

4.3.2 CFD method

In the present study an in-house flow solver, CFD3D, developed by Hein de Vries, is used. The flow solver is based on the finite-volume discretization on unstructured grids. The computational method solves the Reynolds Averaged Navier Stokes equations for time dependent compressible flow (URANS) in a 2D or 3D domain. The discretization is second order accurate both in time and space. A central scheme is employed for the viscous flux. For the convective flux, Roe's scheme upwind based discretization [45] is employed, combined with linear reconstruction of the variables at the faces of the control volume [46]. The discretized equations are integrated in time in an implicit manner. Gauss-Seidel iteration, accelerated by an algebraic multi-grid method, is used to solve the system of linear equations.

For the unsteady flow simulation, an implicit second-order accurate dual time stepping scheme is employed in which a steady state problem is solved in pseudo-time at each physical time step. For temporal convergence, once the sub-iteration residuals drop 4 orders of magnitude or the maximum number of predetermined sub-iterations (here 200) is reached, the solution is advanced to the next physical time step. The solution is advanced at a physical time step of 4.17×10^{-4}s ($\Delta t U_\infty/c = 0.04$). This corresponds to 160 steps per cycle of the actuation. The actuation frequency is 15 Hz in the present case. The CFL number determines the size of the pseudo-time steps. A value of 200 has been used for both the flow equations and the turbulence equations. The turbulence model equations are solved loosely coupled to the flow equations. The order of accuracy of the discretization of the turbulence model equations is equal to that of the flow equations, except for the convective fluxes, which are first order accurate. The two-equation SST k-ω turbulence model [47] is used in the present study. The numerical simulation

is set at fully turbulent mode, i.e. transition occurs close to the leading edge of the airfoil. The numerical flow simulation is started with a steady state flow solution without actuation. Once the steady flow solution is achieved, the actuation is turned on.

4.3.3 Computational Results

Fig. 24 shows during 4 actuation cycles the variation with time of the absolute value of the velocity at the middle of the orifice exit plane. The velocity during the blowing cycle ($0<t/T<0.5$) is more pronounced than the velocity during the suction cycle ($0.5<t/T<1$). The trend is similar to what has been observed from the HWA data, e.g. see Fig. 15a. The predicted velocity history is smoother than the measured one. This might be caused by differences in the actuator. The jet produced in the experiment is the result of a complex acoustic interaction inside a relatively large plenum. The actuator for the numerical simulation is a relatively small, compact cavity with a harmonic motion of its bottom.
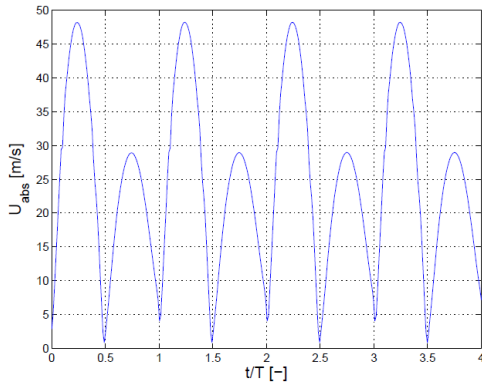

Fig. 24. Predicted velocity in middle of orifice synthetic jet. $\alpha = 0$, Re = 165,000, $M_\infty = 0.045$, $F^+ = 0.16$, $A_p \approx 3.0$

Fig. 25 compares the measured distribution of the pressure coefficient C_p and the predicted distribution from the numerical simulation. The C_p presented is the mean value, i.e. the value averaged over 4 cycles. Clearly the CFD data deviates quite significantly from the experimental data, especially on the bottom side. The pressure data on the top side match satisfactorily, especially downstream of the local disturbance due to the turbulator tape.

The pressure distribution from experiment shows a smaller effect of the actuation than the prediction. However, CFD shows a more distinct effect of the synthetic jet on the pressure distribution, specifically in the region where
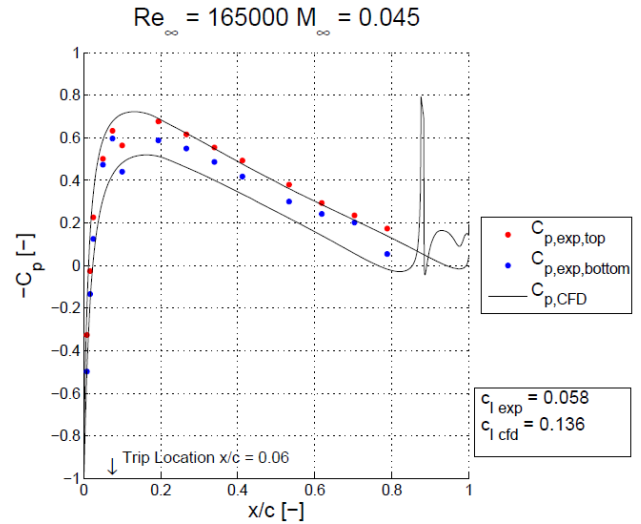

Fig. 25. Comparison of time-averaged pressure distribution from CFD and experiment. $\alpha = 0$, Re = 165,000, $M_\infty = 0.045$, $F^+ = 0.16$, $A_p \approx 3.0$

there are no pressure taps in the model. The predicted lift coefficient from CFD is more than twice that of the experiment, which is also evident from the pressure distribution. Note that the experimental value of c_l is due to the static pressure only, the wall shear stress does not contribute. On the bottom side the pressure distribution shows a strong variation near the trailing edge.
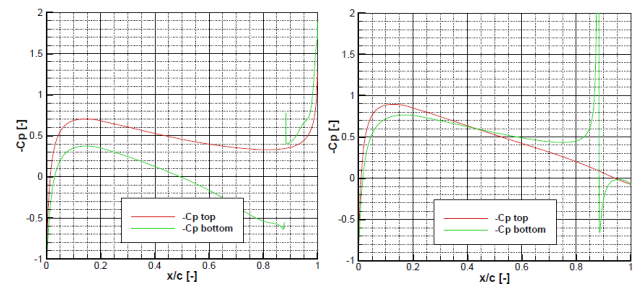

Fig. 26. C_p-distribution during actuation cycle. Left: $t/T = 0.25$ (blowing). Right: $t/T = 0.75$ (suction). $\alpha = 0$, Re = 165,000, $M_\infty = 0.045$, $F^+ = 0.16$, $A_p \approx 3.0$

Fig. 26 shows that during one actuation cycle the C_p-distribution on the lower side shows a strong fluctuation, in particular downstream of

the synthetic jet. The strong fluctuation is related to the vortices shed into the wake during the blowing part of the cycle. The effect of the synthetic jet propagates upstream of the jet on the bottom side and all along the top side, though there the effect is smaller. Near the trailing edge on the top surface, the local effect of the jet on the C_p distribution is seen as the jet develops during the blowing stroke. Fig. 27 shows the time history of the effect of the synthetic jet on the lift coefficient for about 4 cycles of actuation. This shows that the jet induces a mean positive lift enhancement of 0.138 which corresponds to about 1.3 deg pitch angle.
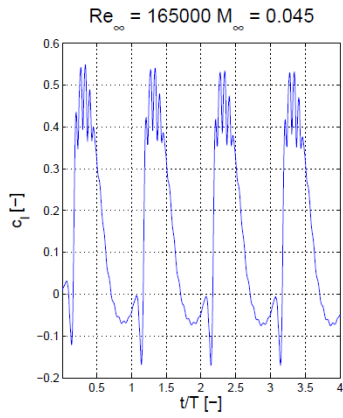

Fig. 27. c_l during 4 actuation cycles. $\alpha = 0$, Re = 165,000, $M_\infty = 0.045$, $F^+ = 0.16$, $A_p \approx 3.0$
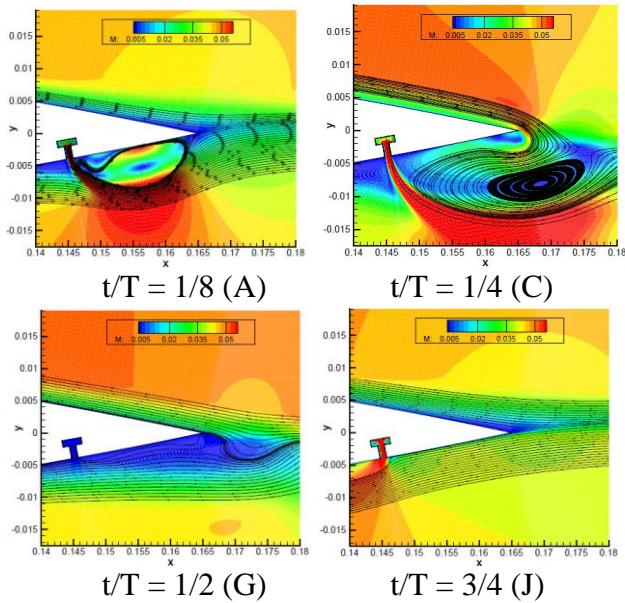

Fig. 28. Instantaneous streamlines and iso-Mach contours in region near trailing edge during actuation cycle. Upper plots: blowing. Lower right: suction. $\alpha = 0$, Re = 165,000, $M_\infty = 0.045$, $F^+ = 0.16$, $A_p \approx 3.0$

A cycle of the synthetic jet consists of half a period blowing followed by half a period suction. The lift history shows fluctuations around the maximum expulsion cycle and a small drop of the lift at the beginning of the cycle.

Fig. 28 shows the evolution of the flow near the trailing edge during 4 instants of the cycle, two during the blowing part of the cycle, one at t/T = 0.5 and one during the suction part of the cycle. Each sub-figure corresponds to a point in Fig. 29, which shows the history of c_l during the whole cycle.
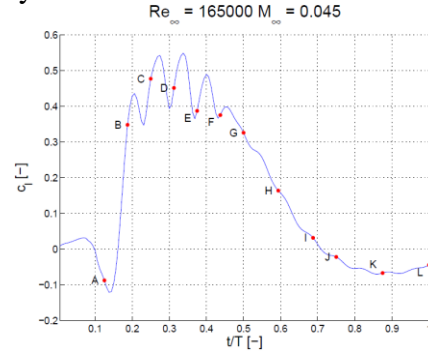

Fig. 29. Evolution of lift coefficient during actuation cycle. Blowing: 0<t/T<0.5. Suction: 0.5<t/T<1. $\alpha = 0$, Re = 165,000, $M_\infty = 0.045$, $F^+ = 0.16$, $A_p \approx 3.0$

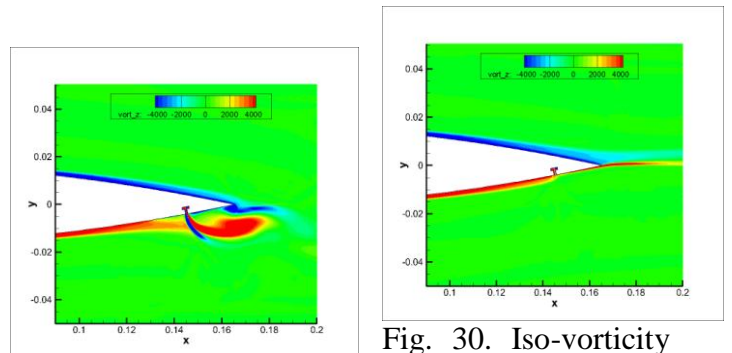Fig. 30 shows the iso-vorticity contours corresponding to two instants in the actuation cycle.

Fig. 30. Iso-vorticity contours in region near trailing edge during actuation cycle. Left: blowing, t/T = 1/4. Right: suction, t/T = 3/4. $\alpha = 0$, Re = 165,000, $M_\infty = 0.045$, $F^+ = 0.16$, $A_p \approx 3.0$

The drop of the lift at the beginning of the cycle can be explained from Fig. 28. At the beginning of the cycle, the jet induces a recirculation region downstream of the jet. However, this recirculation region does not reach the trailing edge and the flow reattaches on the lower surface up-

stream of the trailing edge as clear from the streamline pattern. The recirculation is not strong enough to entrain the flow from the top side of the airfoil. Therefore at the trailing edge the flow is directed along the lower side of the airfoil, which reduces the circulation and therewith the lift. Fig. 28 shows the development of the recirculation region as the jet builds up its strength. The streamlines are clearly deflected downward because of the low pressure area due to the recirculation.

At $t/T = 0.25$ the actuator is at the point of maximum expulsion. It is obvious that the flow from the top side is entrained to the bottom side. This changes the angle at which the flow leaves the trailing edge and increases the circulation. However, this recirculation zone subsequently the recirculation zone is shed into the wake. The shed vortices and the interaction with the flow around the trailing edge cause the lift to show fluctuations, see Fig. 29. There is a sequence of 5 vortices that are shed at the point around the maximum expulsion. Further numerical simulations for lower values of A_p do not show these small fluctuations in lift
At $t/T = 0.75$ the fluid originating from the boundary layer upstream of the orifice is sucked into the plenum. As a result the streamlines are deflected upward resulting in the drop in lift, see Fig. 29.

5 Concluding Remarks

A wind tunnel model with NACA0018 section (c = 0.165 m), equipped with 29 pressure taps, has been tested in a low-speed wind tunnel for Reynolds numbers in the range of 88,000 to 550,000. To eliminate the laminar separation bubble, different turbulator tape thicknesses have been explored. It has been demonstrated that the laminar separation bubble is eliminated using a 0.4 mm thick zig-zag turbulator tape of 0.035c width. The model is equipped with a-coustically-driven synthetic jet, slit width $W/c \sim$ O(0.6%), located on the lower side of the airfoil near the trailing edge ($x/c = 0.88$). Bench-top experiments ($U_\infty = 0$) have provided the param-

eters for which the actuator performs best: peak velocities up to 60 m/s.
The aerodynamic performance has been assessed from the measurement of the surface pressure and from hot-wire anemometry of the velocity inside the synthetic jet, for various Reynolds numbers and angles of attack.
Results of a parametric study have been presented for $\alpha = 0$ and $\alpha = 8$ deg and Re = 165,000 in the low-frequency regime $F^+ \sim$ O(1). It is found that at constant jet strength the effectiveness of the capability to enhance the lift decreases as the frequency increases. At constant frequency, increasing the jet strength increases the control effectiveness of the synthetic jet actuation to change the pitch angle. It is shown that the size of the recirculation zone downstream of the exit of the actuator is proportional to the jet strength and inversely proportional to the actuation frequency.
The control effectiveness of the actuation for $\alpha = 0$ and that for $\alpha = 8$ deg differ, which indicates that the local flow state around the jet affects its performance. This also follows from the comparison of the lift curve for the case with actuation with the one without actuation. A positive effect is observed in the linear regime as well as in the post stall regime.
The positive effect of the jet is accompanied by an increase of the drag of the order 15 - 20 drag counts. The synthetic jets, located on the lower side of the airfoil near the trailing edge, have a strong dynamic effect on the pressure distribution on the lower side upstream of the jet and a smaller dynamic effect on the upper side.
Results of numerical flow simulations, employing an URANS computational method, have given much insight in the details of the physics of the low-frequency actuation.
The numerical flow simulations reveal that fluctuations in the lift and the drag correlate to the recirculation zone being shed into the wake periodically, directly affecting the direction at which the flow leaves the airfoil at the trailing edge, i.e. the "Kutta condition".
Comparison of numerical results with experimental results show significant differences for the test case considered: $\alpha = 0$, $F^+ = 0.16$, Re = 165,000 and peak velocity ratio $A_p \approx 3.0$.

References

[1] S.J. Johnson, J.P. Baker, CP van Dam, and D. Berg. An overview of active load control techniques for wind turbines with an emphasis on microtabs. *Wind Energy*, 13(2-3):239–253, 2010.

[2] P.C. Pennings. *Development of an experiment for leading edge active fluidic flow control of a wind turbine airfoil.* MSc thesis, University of Twente, 2011.

[3] E.A. Mayda, C.P. van Dam, and D.T Yen-Nakafuji. Computational investigation of finite width microtabs for aerodynamic load control. *AIAA Paper*, 2005-*1185*, 2005.

[4] M. Blaylock, R. Chow, and C.P. van Dam. Comparison of microjets with microtabs for active aerodynamic load control. *AIAA Paper 2010-4409*, 2010

[5] C.S. Boeije, H. de Vries, I. Cleine, E. van Emden, G.G.M. Zwart, H. Stobbe, A. Hirschberg, and H.W.M. Hoeijmakers. Fluidic load control for wind turbine blades. *AIAA Paper 2009-684*, 2009

[6] P. Baek, M. Gaunaa, N. N. Sorensen, and P. Fulgsang. A comparison of Two devices for distributed active load control of wind turbine blades. In *TORQUE 2010: The Science of Making Torque from Wind*, June 28-30, Crete, Greece, pages 611–617, 2010.

[7] A. M. Cooperman, R. Chow, S. J. Johnson, and C.P. van Dam. Experimental and computational analysis of a wind turbine airfoil with active microtabs. *AIAA Paper 2011-347*, 2011.

[8] R. Chow and C.P. van Dam. Unsteady computational investigations of deploying load control microtabs. *Journal of Aircraft*, 43(5):1458–1469, 2006.

[9] J.P. Baker, K.J. Standish, and C.P. van Dam. Two-dimensional wind tunnel and computational investigation of a microtab modified airfoil. *Journal of Aircraft*, 44(2):563–572, 2007.

[10] R.C.J. Lindeboom, J.J.H.M. Sterenborg, and C.J. Simao Ferreira. Determination of unsteady loads on a DU96W180 airfoil with actuated flap using particle image velocimetry. *TORQUE 2010 : The Science of Making Torque from Wind*, June 28-30, Crete, Greece, pages 113–126, 2010.

[11] Mohamed Gad el Hak. *Flow control:passive, active, and reactive flow management*. Cambridge University Press, 1st edition, 2000.

[12] S. S. Collis, R. D. Joslin, A. Seifert, and V. Theofilis. Issues in active flow control: theory, control, simulation, and experiment. *Progress in Aerospace Sciences*, 40(4-5):237–289, 2004.

[13] D. Greenblatt and I. J. Wygnanski. The control of flow separation by periodic excitation. *Progress in Aerospace Sciences*, 36(7):487–545, 2000.

[14] I. J. Wygnanski. The variables affecting the control of separation by periodic excitation. *AIAA Paper 2004-2505*, 2004.

[15] C.S. Boeije. *Exploratory study of fluidic control of pitch angle and flow separation for a wind turbine airfoil.* MSc thesis, Universiteit of Twente, 2008.

[16] D.M. DeSalvo and A. Glezer. Aerodynamic performance modification at low angles of attack by trailing edge vortices. In 2nd *AIAA Flow Control Conference.*, Portland, OR, pages 28–31, 2004.

[17] J. M. Thomas. *Numerical simulation of active flow control on airfoils*. MSc thesis, Universiteit Twente, 2010.

[18] T.J. Mueller and J.D. DeLaurier. Aerodynamics of small vehicles. *Annual Review of Fluid Mechanics*, 35(1):89–111, 2003.

[19] A. Glezer and M. Amitay. Synthetic jets. *Annual Review of Fluid Mechanics*, 34(1):503–529, 2002.

[20] L. N. Cattafesta and M. Sheplak. Actuators for active flow control. *Annual Review of Fluid Mechanics*, 43:247–272, 2011.

[21] R. Mittal and P. Rampunggoon. On the virtual aeroshaping effect of synthetic jets. *Physics of Fluids*, 14:1533, 2002.

[22] M. Amitay and A. Glezer. Aerodynamic flow control using synthetic jet actuators. *Control of Fluid Flow*, pages 45–73, 2006.

[23] M. Amitay and A. Glezer. Role of actuation frequency in controlled flow reattachment over a stalled airfoil. *AIAA Journal*, 40(2), 2002.

[24] J.A. Franck and T. Colonius. Oscillatory control and the effects of actuation frequency on a wall-mounted hump model, *AIAA Paper 2009-4019*, 2009.

[25] S. Abdou and S. Ziada. Spanwise characteristics of high-aspect-ratio synthetic jets. *AIAA Journal*, 44(7):1516–1523, 2006.

[26] R. Petz and W. Nitsche. Designing actuators for active separation control experiments on high-lift configurations. *Active Flow Control*, pages 69–84, 2007.

[27] J. L. Gilarranz, L. W. Traub, and O. K. Rediniotis. A new class of synthetic jet actuators—Part II: application to flow separation control. *Journal of Fluids Engineering*, 127(2):377–387, 2005.

[28] J. L. Gilarranz, L. W. Traub, and O. K. Rediniotis. A new class of synthetic jet actuators—Part I: design, fabrication and bench top characterization. *Journal of Fluids Engineering*, 127(2):367–376, 2005.

[29] A. Tuck and J. Soria. Active flow control of a NACA 0015 airfoil using a ZNMF jet. In *Australian Aerospace Student Conference*, Sydney, 2004.

[30] V. Maldonado, J. Farnsworth, W. Gressick, and M. Amitay. Active enhancement of wind turbine blade performance. *AIAA Paper 2008-1311*, 2008.

[31] M. Jabbal and S. Zhong. The near wall effect of synthetic jets in a boundary layer. *International Journal of Heat and Fluid Flow*, 29(1):119–130, 2008.

[32] O. Stalnov, A. Kribus, and A. Seifert. Evaluation of active flow control applied to wind turbine blade section. *Journal of Renewable and Sustainable Energy*, 2:063101, 2010.

[33] S. G. Mallinson, J. A. Reizes, G. Hong, and P. S. Westbury. Analysis of hot-wire anemometry data obtained in a synthetic jet flow. *Experimental Thermal and Fluid Science*, 28(4):265–272, 2004.

[34] L. Oren, J. Cha, E. Gutmark, and S. Khosla. Instability process in synthetic jets. *AIAA Paper 2011-33*, 2011.

[35] A. Seifert and LG Pack. Oscillatory control of separation at high Reynolds numbers. *AIAA journal*, 37(9), 1999.

[36] D. Greenblatt and I. Wygnanski. Effect of leading-edge curvature on airfoil separation control. *Journal of Aircraft*, 40(3):473–481, 2003.

[37] R. Petz and W. Nitsche. Active separation control on the flap of a two-dimensional generic high-lift configuration. *Journal of Aircraft*, 44(3):865–874, 2007.

[38] P. Scholz, S.S. Mahmood, M. Casper, R. Radespiel, M. Sitzmann, and V. Ciobaca. Experimental and numerical investigations on the control of airfoil stall using vortex generator jets. *AIAA Paper 2010-4250*, 2010.

[39] Immanuel Geesing. Private Communication. 2011.

[40] Klaas Bootsma. *De invloed van turbulatoren op de grenslaag van een profiel van een windturbine blad*. BSc Assignment, University of Twente, 2011.

[41] M.A. Mitay, D.R. Smith, V. Kibens, D.E. Parekh, and A. Glezer. Aerodynamic flow control over an unconventional airfoil using synthetic jet actuators. *AIAA Journal*, 39(3):361–370, 2001.

[42] B.L. Smith and A. Glezer. The formation and evolution of synthetic jets. *Physics of Fluids*, 10:2281, 1998.

[43] C. Geuzaine and J.F. Remacle. Gmsh: A 3-D finite element mesh generator with built-in pre-and post-processing facilities. *International Journal for Numerical Methods in Engineering*, 79(11):1309–1331, 2009.

[44] S.M.D. Widjanarko. *Active aero-fluidic load control on wind turbine blades*. MSc thesis, University of Twente, 2011.

[45] P.L. Roe. Approximate Riemann solvers, parameters vectors, and difference schemes. *Journal of Computational Physics*, Vol. 43, pp. 357 – 372, 1981.

[46] B. van Leer. Towards the ultimate conservative difference scheme, V. A second order sequel to Godunov's method. *Journal of Computational Physics*, Vol. 32, pp. 101 – 136, 1979.

[47] F.R. Menter. *Improved two-equation k-ω turbulence models for aerodynamic flows*. NASA TM 103975, 1992.

Copyright Statement